Structures of $M^+(CH_4)_n$ (M=Ti,V) Based on Vibrational Spectroscopy and Density Functional Theory

Justine Kozubal, Tristan Heck, and Ricardo B. Metz*

Department of Chemistry, University of Massachusetts, Amherst

Amherst, Massachusetts 01003, United States

E-mail: rbmetz@chem.umass.edu

Phone: +1-413-545-6089. Fax: +1-413-545-4490

Abstract

Photofragment spectroscopy is used to measure the vibrational spectra of $M^+(CH_4)(Ar)$ and $M^+(CH_4)_n$ (M=Ti,V; n=1-4) in the C−H stretching region (2550-3100 cm^{-1}). Spectra were measured by monitoring loss of Ar from $M^+(CH_4)(Ar)$ and loss of CH_4 from the larger clusters. The experimental spectra are then compared to simulations done at the B3LYP/6-311++G(3df,3pd) level of theory to identify the structures of the ions. The spectra all have a peak near 2800 cm^{-1} due to the symmetric C−H stretch of the hydrogens adjacent to the metal. Some complexes also have a smaller peak due to the corresponding antisymmetric stretch. Most complexes also have a peak near 3000 cm^{-1} due to the C−H stretch of hydrogens pointing away from the metal. The symmetric proximate C−H stretches of $M^+(CH_4)(Ar)$ to $M^+(CH_4)_4$ are red shifted from the symmetric stretch in bare CH_4 by 149, 152, 128, and 107 cm^{-1} for the titanium complexes and 164, 175, 158, and 146 cm^{-1} for the vanadium complexes. In $M^+(CH_4)(Ar)$ (M=Ti,V), the heavy atoms are collinear. $Ti^+(CH_4)(Ar)$ has η^3 methane hydrogen coordination ($\angle$M−C−H=180°), while $V^+(CH_4)(Ar)$ has η^2 ($\angle$M−C−H=124°). The n=2 complexes have C−M−C linear. $Ti^+(CH_4)_2$ has C_{2h} symmetry with η^3 CH_4 while $V^+(CH_4)_2$ has methane coordination intermediate between η^2 and η^3 ($\angle$M−C−H=156°). Both the $M^+(CH_4)_3$ (M=Ti,V) complexes have C_{2v} symmetry with one methane farther away from the metal in an η^2 binding orientation and two methanes close to the metal with a nearly η^2 methane for vanadium and coordination between η^2 and η^3 CH_4 for titanium ($\angle$M−C−H=150°). In $Ti^+(CH_4)_4$ and $V^+(CH_4)_4$ all of the methanes have η^2 coordination. The titanium complex has a distorted square planar geometry with two different Ti-C bond lengths and the vanadium complex is square planar.

1 Introduction

Methane, from natural gas, is widely used for electricity generation and heating. However, because it is a permanent gas, its use as a transportation fuel is limited.[1] Industrially, methane can be converted to liquid hydrocarbons by steam reforming to produce synthesis gas, followed by Fischer-Tropsch synthesis.[2,3] However, this indirect process is highly energy intensive. As a result, an alternative, direct process to convert methane to a liquid fuel has long been a goal of catalysis.[2,4]

Activation of methane by gas-phase metal ions $M^+ + CH_4 \longrightarrow MCH_2{}^+ + H_2$ is exothermic and occurs under thermal conditions for several of the 5d transition metals, M=Ta, W, Os, Ir, Pt, while it is endothermic for the 3d and 4d metals (although it is nearly thermoneutral for Zr and Nb).[5–15] Gas-phase metal cations are thus an excellent system in which to study methane activation as they exhibit the desired reactivity; they have been studied in detail by experiment and theory (see refs.[16–19] and references therein).

Several groups have studied the reactions of Ti^+ and V^+ with methane. In single-collision, guided ion beam studies, Armentrout and coworkers determined that dehydrogenation of methane by Ti^+ and V^+ is endothermic by ∼70 kJ/mol and ∼125 kJ/mol, respectively.[20,21] By measuring the reactions with different source conditions, they were able to estimate the reactivities of specific electronic states. They concluded that electronically excited, low-spin Ti^+ and V^+ react readily with methane. A recent paper by Ng *et al.* studied reactions of electronic and spin-orbit state selected V^+. They determined the triplet $V^+(a^3F_J)$ ion has an order of magnitude higher reactivity with methane than the quintet (a^5D_J) and (a^5F_J) states, indicating that the lowest energy pathway is on the triplet surface and that quintet-to-triplet spin crossing is inefficient.[22]

At room temperature, under multiple-collision conditions in 0.75 Torr of helium buffer gas, Tonkyn *et al.* noted that Ti^+ forms adducts with up to five CH_4. No dehydrogenation reactions were observed.[23] This was confirmed in later work by Shayesteh *et al.*, who only observed $M^+(CH_4)_{1,2}$ adduct formation in thermal reactions of Ti^+ and V^+ with methane in

0.35 Torr helium.[14] van Koppen *et al.* reacted Ti^+ with 2.2 Torr of methane and observed production of $Ti^+(CH_4)_n$ (n=1-5). Above ∼500 K they also observe dehydrogenation of clusters with n=3, indicating the onset of C−H bond activation.[24,25]

The intermediates and products of the reactions of *neutral* titanium and vanadium atoms with methane have been studied using IR spectroscopy, in a cryogenic matrix. Bihlmeier *et al.*[26] found that upon photo-excitation, Ti inserts into the C−H bond, forming H-Ti-CH_3. Andrews *et al.* studied matrix infrared spectra of reaction products of Ti and V with CH_4. With titanium, they also observe the insertion product H-Ti-CH_3, which then goes on to form CH_2=TiH_2. It can react with a second methane to produce $(CH_3)_2TiH_2$.[27] For vanadium, only the monohydrido methyl complex, H-V-CH_3, is formed.[28]

In investigating $M^+(CH_4)_n$ complexes, two key questions are:
What is the structure of the complex?
To what extent does the interaction with the metal weaken the C−H bonds in methane?
Vibrational spectroscopy, particularly in the C−H stretching region, is an excellent tool to address these questions. Vibrational spectroscopy has been used to study $Li^+(CH_4)Ar_{1\text{-}6}$,[29] $Li^+(CH_4)_{1\text{-}9}$,[30] $Al^+(CH_4)_{1\text{-}6}$,[31] $Mn^+(CH_4)_{1\text{-}6}$,[32] $Zr^+(CH_4)_{1\text{-}4}$,[33] and the late transition metals $Fe^+(CH_4)_{1\text{-}4}$,[34] $Co^+(CH_4)_{1\text{-}4}$,[35] $Ni^+(CH_4)_{1\text{-}4}$,[35] $Cu^+(CH_4)_{1\text{-}6}$,[36] $Ag^+(CH_4)_{1\text{-}6}$,[36] $Pt^+(CH_4)_{1\text{-}4}$,[37] and $Au^+(CH_4)_{3\text{-}8}$.[38] Electronic spectroscopy has been used to study $Mg^+(CH_4)$,[39] $Ca^+(CH_4)$,[40] $V^+(CH_4)$,[41] and $Zn^+(CH_4)$,[42] primarily characterizing the metal-methane stretches and bends in excited electronic states.

Previous spectroscopy of $M^+(CH_4)_n$ has focused on the late transition metals. The early transition metal cations provide an interesting contrast, as they have low-lying d^n and $d^{n-1}s$ electronic states with the same spin multiplicity, leading to facile s-d hybridization. In this study, we report vibrational spectra of $Ti^+(CH_4)(Ar)$, $Ti^+(CH_4)_n$ (n=2-4), $V^+(CH_4)(Ar)$, and $V^+(CH_4)_n$ (n=2-4) complexes measured via photofragment spectroscopy. The experimental results are compared with simulations to determine the geometry of the molecules.

2 Methods

The molecules are produced in a laser ablation source and their spectra are measured on a home-built dual time-of-flight reflectron mass spectrometer[43] coupled to an IR laser system. The $M^+(CH_4)(Ar)$ and $M^+(CH_4)_{2\text{-}4}$ (M=Ti,V) complexes are produced by ablating a metal rod that is continuously translating and rotating using the second harmonic (532 nm) of a Nd:YAG laser operating at 7 mJ/pulse with a repetition rate of 20 Hz. Just before the laser fires, a pulse of gas is introduced through a valve (General Valve, Series 9). The ions then travel through a 11 mm long, 2.5 mm ID tube after laser ablation. A longer tube (42 mm) was used to take the spectra of $V^+(CH_4)_4$ and is described in detail elsewhere.[33]

For $Ti^+(CH_4)_n$ (n=2-4), the gas mixture is 5% CH_4 in He at a backing pressure of 80-100 psi. $Ti^+(CH_4)(Ar)$ is made with 0.25% CH_4 and 10% Ar in He at 80 psi. The gas mix is 0.6% CH_4 and 20% Ar in He at 90 psi for $V^+(CH_4)(Ar)$, 10% CH_4 in He at 70 and 30 psi, respectively, for $V^+(CH_4)_n$ (n=2, 3), and 100% He at 30 psi in the primary valve and 100% CH_4 at 15 psi in the secondary valve for $V^+(CH_4)_4$.[33]

Ions then expand into vacuum and cool, creating a molecular beam whose rotational temperature is $\sim$15 K.[44] The ion beam is skimmed, extracted into the time-of-flight mass spectrometer, accelerated, and re-referenced to ground potential. The ions are then mass selected and, at the turning point of the reflectron, irradiated by a Nd:YAG-pumped OPO/OPA IR laser system (LaserVision). The laser produces 7-9 mJ/pulse near 3000 cm^{-1}, with a line width of 1.8 cm^{-1}; its wavelength is calibrated using the absorption spectrum of methane.[45] The dissociation yield is increased by multipassing the laser beam about 21 times through the ion cloud using two curved mirrors.[46]

The parent and photofragment ions separate in the second time-of-flight stage and are collected on a 40 mm dual microchannel plate detector, allowing their masses to be determined from their flight times. The resulting ion signals are amplified and collected on a gated integrator and a *LabView* based program is used to record the data. The photodissociation spectrum is obtained by normalizing the fragment signal to the parent signal and laser

power as a function of wavelength. The observed fragments correspond to loss of Ar from $M^+(CH_4)(Ar)$ (M=Ti,V) and one or more intact CH_4 from $M^+(CH_4)_n$ (M=Ti,V; n=2-4).

Calculations are carried out with the *Gaussian09* program package.[47] Optimized geometries of the ions are calculated using the B3LYP and M11L[48] density functionals and the 6-311++G(3df,3pd) basis set. Vibrational frequencies are scaled by 0.964 (B3LYP) and 0.972 (M11L) based on the ratio of the experimental and computed values of the symmetric and antisymmetric C−H stretching frequencies of CH_4. All reported energies include unscaled zero-point energies. Simulated spectra are calculated by convoluting the calculated stick spectrum with a Gaussian with 20 cm^{-1} FWHM.

3 Results & Discussion

Photofragment spectroscopy is used to measure the spectra of the entrance channel complexes $M^+(CH_4)(Ar)$ and $M^+(CH_4)_n$ (M=Ti,V; n=2-4) in the C−H stretching region 2550-3100 cm^{-1}. Argon tagging is used for the smallest complexes because the CH_4 binding energy exceeds the photon energy and infrared multiple-photon dissociation (IRMPD) is inefficient for ions this small.[37]

The C−H stretching frequencies and intensities depend on how many hydrogens coordinate to the metal. For cations, the two limiting cases are η^2 hydrogen coordination, which corresponds to C_{2v} symmetry in an $M^+(CH_4)$ complex, and η^3 hydrogen coordination, which has C_{3v} symmetry. Because the coordination can be between η^2 and η^3, it is useful to specify the angle between the metal, carbon, and the hydrogen farthest from the metal. Then, ∠M−C−H∼124° for η^2 coordination and 180° for η^3 coordination. The spectra, structures, and corresponding simulations of the $Ti^+(CH_4)_n$ complexes will be discussed in Section 3.2, followed by the $V^+(CH_4)_n$ complexes in Section 3.3.

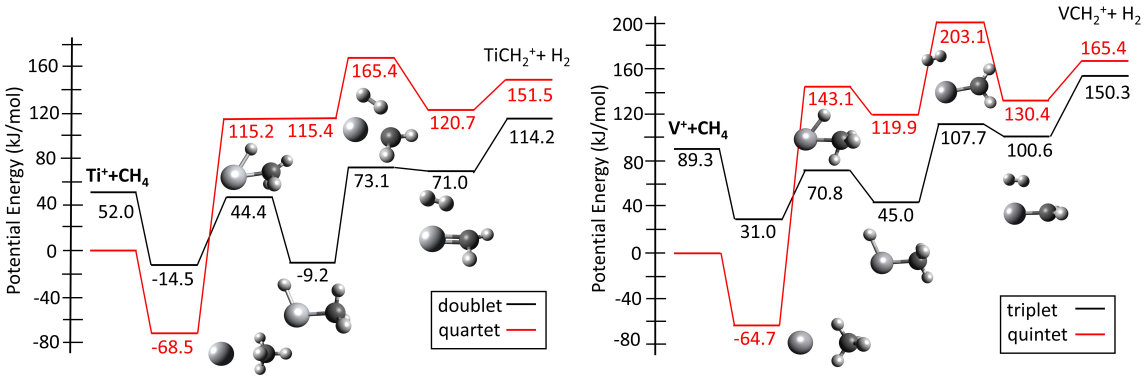

Figure 1: High-spin (red) and low-spin (black) potential energy surfaces for the reaction of Ti^+ and V^+ with CH_4 at the B3LYP/6-311++G(3df,3pd) level of theory. Only the lowest energy geometries are shown, the rest can be found in Tables S2 and S3.

Table 1: M^+-L (M=Ti,V) and Methane Bond Dissociation Energies, in kJ/mol, to ground state products

Species	S[a]	B3LYP[b]	M11L[b]	Experiment
Ti^+ splitting[c]		52.0	65.9	54.5
Ti^+-H	3	231.3	209.8	223 ± 11[d,m]
Ti^+-H_2	4	41.1	28.6	31 ± 2[e]
Ti^+-CH	1	414.4	393.3	478 ± 5[f,g,m]
Ti^+-CH_2	2	336.4	340.4	380 ± 9[f,m]
Ti^+-CH_3	3	228.4	220.5	214 ± 3[g,m]
V^+ splitting[c]		89.3	29.5	104.0
V^+-H	2	124.8	151.0	195 ± 5[h,m]
V^+-H_2	5	47.6	33.5	43 ± 2[i]
V^+-CH	2	391.3	431.5	470 ± 5[j,k,m]
V^+-CH_2	3	300.2	350.1	328 ± 7[h,m]
V^+-CH_3	2	125.5	177.2	200 ± 9[h,m]
CH_3-H	1	425.2	433.3	432.46 ± 0.03[l]
CH_2-H_2	1	450.6	454.0	457.62 ± 0.10[l]

[a]Multiplicity [b]Calculations use the 6-311++G(3df,3pd) basis set, are at zero Kelvin and include zero point energy [c]Splittings are the energy of the lowest low-spin excited state relative to the high-spin ground state. Experimental splittings are the spin-orbit weighted average. [d]Ref.[49] [e]Ref.[50] [f]Ref.[51] [g]Ref.[52] [h]Ref.[22] [i]Ref.[53] [j]Ref.[54] [k]Ref.[21] [l]Ref.[55] [m]Ref.[56]

3.1 PES

Figure 1 shows the potential energy surfaces for the reactions of Ti^+ and V^+ with CH_4. In each case, the ground state of the reactants and the $M^+(CH_4)$ entrance channel complex is high spin. There is a substantial barrier to C−H bond activation and formation of a $[H-M-CH_3]^+$ insertion intermediate. In the lowest energy pathway this transition state and all subsequent intermediates and products are lower spin than the reactants. There is an additional intermediate, the $(H_2)MCH_2^+$ exit channel complex, which can then dissociate to form the $MCH_2^+ + H_2$ products. The overall dehydrogenation reaction is significantly endothermic. These potential energy surfaces are similar to those calculated by Russo and Sicilia[57] and are consistent with the measured thermochemistry shown in Table 1. Under our experimental conditions, we only expect to make the high spin $M^+(CH_4)$ (M=Ti,V) entrance channel complexes.

3.2 $Ti^+(CH_4)_n$

The experimental spectra of $Ti^+(CH_4)(Ar)$ and $Ti^+(CH_4)_n$ (n=2-4) in Figure 2 show peaks to the red of the symmetric C−H stretch in bare CH_4 (2917 cm^{-1}) and a peak around 3000 cm^{-1}, near the position of the CH_4 antisymmetric stretch (3019 cm^{-1}). The intensity of the peak around 3000 cm^{-1} decreases as more CH_4 molecules are added to the metal, and completely disappears for n=4. This suggests the methane binding to the metal changes its orientation as more methanes are added.

3.2.1 $Ti^+(CH_4)(Ar)$

$Ti^+(CH_4)$ has a calculated binding energy of 5732 cm^{-1} (Table 2) so it requires more than one photon to dissociate. Infrared multiple-photon dissociation is inefficient for molecules this small, but a spectrum was obtained despite the low dissociation yield. The spectrum (Figure S1) shows a weak peak at 2768 cm^{-1} and a more intense peak at 3014 cm^{-1}. In $Ti^+(CH_4)(Ar)$ the Ar tag has a calculated binding energy of 2524 cm^{-1}. Its spectrum (Figure

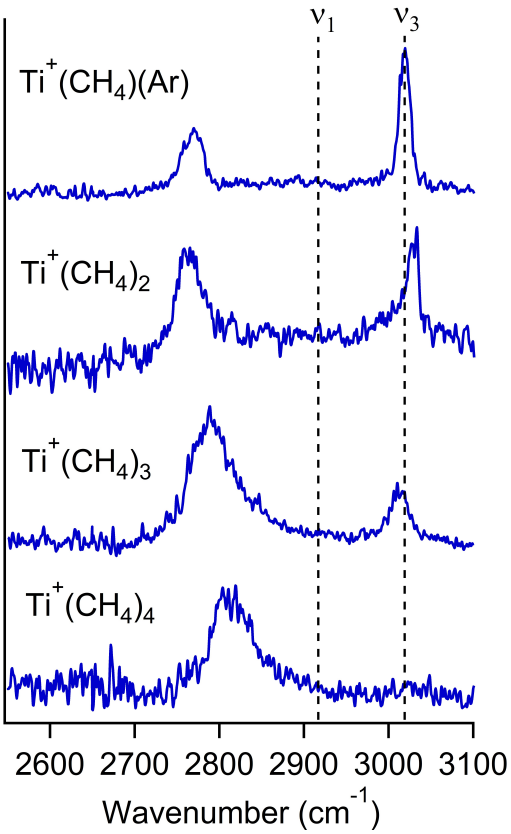

Figure 2: Vibrational spectra of $Ti^+(CH_4)(Ar)$ and $Ti^+(CH_4)_n$ n=2-4 in the C−H stretching region 2550-3100 cm^{-1}. The symmetric (ν_1) and antisymmetric (ν_3) stretches in bare CH_4 are shown by the dotted vertical lines. The y-axis shows the normalized photofragment yield.

Table 2: Experimental and calculated binding energies of $Ti^+(CH_4)(Ar)$ and $Ti^+(CH_4)_n$ n=1-4[a]

Species	cm^{-1}	kJ/mol	exp (kJ/mol)
Ti^+-CH_4	5732	68.6	70.3±2.5[b]
Ti^+CH_4-Ar	2524	30.2	
$Ti^+CH_4-CH_4$	4832	57.8	72.8±2.5[b]
$Ti^+(CH_4)_2-CH_4$	1174	14.0	27.6±6.3[b]
$Ti^+(CH_4)_3-CH_4$	1649	19.7	41.0±3.3[b]

[a]Calculations are at zero Kelvin at the B3LYP/6-311++G(3df,3pd) level of theory. [b]Ref.[25]

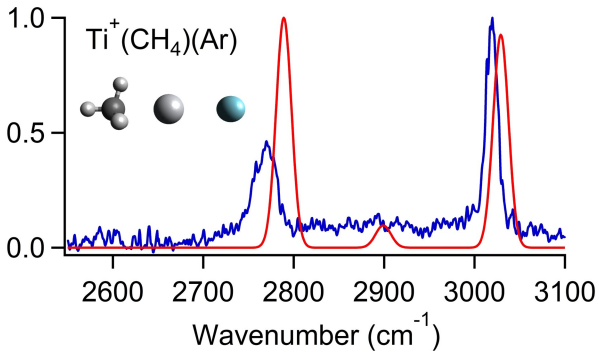

Figure 3: Experimental photodissociation spectrum (blue), simulated spectrum (red), and the optimized geometry of $Ti^+(CH_4)(Ar)$ at the B3LYP/6-311++G(3df,3pd) level of theory.

3) has better signal to noise and is very similar to that of the untagged molecule, with a medium-intensity peak at 2770 cm^{-1} and a more intense peak at 3020 cm^{-1}.

In their study of the binding energies of $Ti^+(CH_4)_n$ (n=1-5) van Koppen *et al.*[25] calculated structures for n=1-3 with the B3LYP functional and Hay/Wadt basis on Ti and 6-31G(d,p) on C and H. Our calculations, which use the same functional and a larger basis set, give very similar results. The $Ti^+(CH_4)$ molecule is calculated to have η^3 methane hydrogen coordination and r_{Ti-C}=2.351 Å. The calculated Ti^+-CH_4 binding energy of 68.6 kJ/mol is in excellent agreement with the measured[25] value of 70.3±2.5 kJ/mol. For $Ti^+(CH_4)(Ar)$, the calculations predict the Ar−Ti−C atoms are collinear and the CH_4 retains η^3 hydrogen coordination. The computed Ti−C bond length is 2.367 Å, which is only 0.016 Å longer than in the untagged complex. The calculations predict similar peak positions ($\leq$4 cm^{-1} shifts) for the C−H stretches of the untagged and tagged complexes, confirming that the Ar only has a small effect on the spectrum. The ground state of Ti^+ is a quartet, and it remains so with the addition of Ar and at least four CH_4.

The simulated spectrum has two almost equally intense peaks at 2789 and 3029 cm^{-1} and a very weak peak at 2899 cm^{-1}. The peak at 2789 cm^{-1} corresponds to the symmetric proximate C−H stretch, while the peak at 3029 cm^{-1} corresponds to the free distal C−H stretch. The peak at 2899 cm^{-1} is the doubly degenerate antisymmetric C−H stretch and is not seen in the experimental spectrum. The experimental peaks (2770 and 3020 cm^{-1}) are

sharp and slightly more red shifted than predicted.

3.2.2 $Ti^+(CH_4)_2$

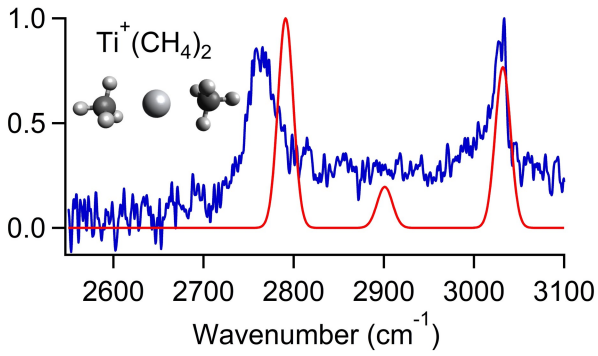

Figure 4: Experimental photodissociation spectrum (blue), simulated spectrum (red), and the optimized geometry of $Ti^+(CH_4)_2$ at the B3LYP/6-311++G(3df,3pd) level of theory.

Although the second CH_4 is predicted to be bound by 4832 cm^{-1}, $Ti^+(CH_4)_2$ photodissociates readily. The experimental spectrum, shown in Figure 4, has two intense peaks, at 2765 and 3034 cm^{-1}. The moderate photodissociation yield we observe is consistent with absorption of two photons being required for photodissociation, in agreement with the calculated binding energy. However, the experimental binding energy[25] of 6090 ± 210 cm^{-1} is likely slightly high, as it would require absorption of three photons, which would lead to less dissociation than is observed. The calculations predict the C−Ti−C atoms are collinear and the Ti−C bond lengths are 2.373 Å. The molecule has C_{2h} symmetry - the methanes have η^3 hydrogen coordination and the hydrogens on the two methanes are staggered by 60°. This is in agreement with the results of van Koppen *et al.*[25] The simulated spectrum consists of two intense peaks at 2791 and 3032 cm^{-1} which are due to the symmetric proximate C−H stretch and the free distal C−H stretch, respectively. There is a weak peak at 2901 cm^{-1} which corresponds to two antisymmetric C−H stretches and is not seen in the experimental spectrum. There is, however, some dissociation in this region so the baseline is not zero. The predicted position of the symmetric stretch peak is 26 cm^{-1} too high, while the simulation captures the position of the free C−H stretch well.

3.2.3 $Ti^+(CH_4)_3$

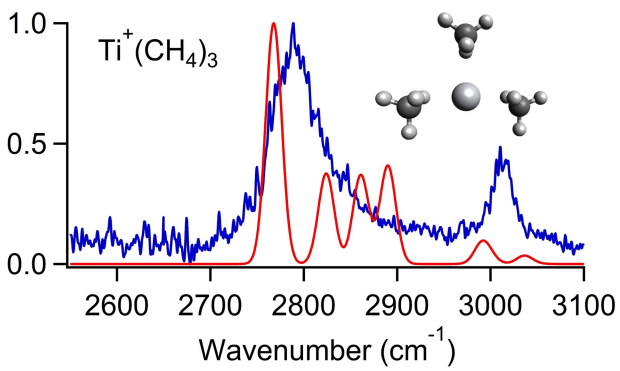

Figure 5: Experimental photodissociation spectrum (blue), simulated spectrum (red), and the optimized geometry of $Ti^+(CH_4)_3$ at the B3LYP/6-311++G(3df,3pd) level of theory.

The calculations predict that the third CH_4 is bound to the metal by only 1174 cm^{-1} which is much weaker than the first two ligands; experiments by van Koppen *et al.*[25] give a slightly higher value, 2300 ± 500 cm^{-1}. The experimental spectrum of $Ti^+(CH_4)_3$ (Figure 5) consists of an intense and fairly broad peak at 2789 cm^{-1} and a much smaller, narrower peak at 3010 cm^{-1}.

The calculated structure of $Ti^+(CH_4)_3$ has near C_{2v} symmetry, with two methanes close to the metal, with r_{Ti-C}=2.483 Å and ∠C−Ti−C=160°. The third methane is much further from the metal, with r_{Ti-C}=2.733 Å.[25] The first two methanes have hydrogen coordination intermediate between η^2 and η^3 (∠Ti−C−H=150°), while the third has η^2 coordination. The simulated spectrum (Figure 5) has an intense peak at 2768 cm^{-1} due to the symmetric proximate C−H stretches of the two closer methanes; the corresponding peak for the more distant methane is at 2824 cm^{-1}. The analogous antisymmetric C−H stretch peaks are at 2861 cm^{-1} (close CH_4) and 2890 cm^{-1} (distant CH_4). The distal C−H stretches give rise to the small peaks at 2991 and 3036 cm^{-1}. The experimental spectrum does not show separate peaks for the two types of methanes. Rather, it consists of an intense, broad peak in the region of the symmetric proximate C−H stretches and a narrower peak in the region of the distal C−H stretches. The observed spectrum is consistent with a dynamic structure, with

the three methanes inter-converting rapidly over a small barrier. This is very similar to what was observed for $Zr^+(CH_4)_3$.[33]

3.2.4 $Ti^+(CH_4)_4$

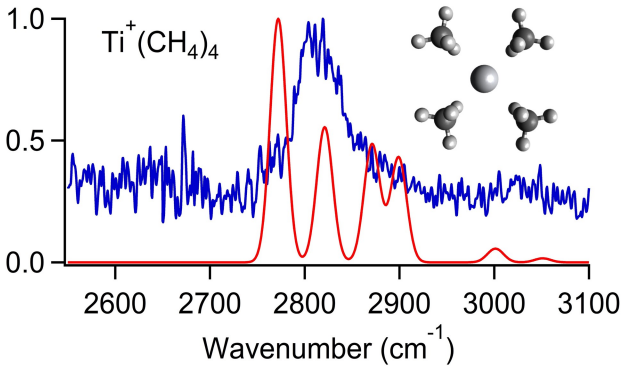

Figure 6: Experimental photodissociation spectrum (blue), simulated spectrum (red), and the optimized geometry of $Ti^+(CH_4)_4$ at the B3LYP/6-311++G(3df,3pd) level of theory.

The fourth CH_4 is calculated to be bound by 1649 cm^{-1}, which is slightly stronger than the third. This is supported by the experiments of van Koppen *et al.*[25] (Table 2). This trend has also been observed for $Zr^+(CH_4)_n$ complexes.[33] The experimental spectrum of $Ti^+(CH_4)_4$ (Figure 6) consists of a broad, intense peak at 2810 cm^{-1}. The lowest energy isomer has a distorted square planar structure in which two Ti−C bond lengths are 2.562 Å and two are 2.725 Å. All four CH_4 are in an η^2 orientation, which explains the absence of a peak around 3000 cm^{-1}. The square planar geometry is only 145 cm^{-1} higher in energy with r_{Ti-C}=2.690 Å and η^2 CH_4, but it is not a local minimum. The simulated spectrum predicts peaks due to the proximate symmetric C−H stretches of the nearby and more distant methanes at 2772 and 2821 cm^{-1} respectively. The analogous proximate antisymmetric C−H stretches are at 2871 and 2899 cm^{-1}. Again, the observed spectrum, which consists of a single, broad peak, is consistent with a dynamic structure, with the nearby and more distant methanes exchanging position rapidly over a low barrier.

3.2.5 $Ti^+(CH_4)_n$ vs. $Zr^+(CH_4)_n$

The experimental spectra of the entrance channel complexes for reaction of Ti^+ and isoelectronic Zr^+ with methane are shown side by side in Figure S2. The $Ti^+(CH_4)(Ar)$ and $Ti^+(CH_4)_2$ spectra have similar peak positions to those of $Zr^+(CH_4)(Ar)$ and $Zr^+(CH_4)_2$.[33] Despite having similar binding energies, the spectra of the Zr^+ complexes are much broader and noisier than those of the Ti^+ species. The peak positions for the symmetric C−H stretch for these two sets of molecules are within 15 cm^{-1} of each other. Although the spectra of $M^+(CH_4)_3$ are similar, the C−H symmetric stretch in $Zr^+(CH_4)_3$ is red shifted 42 cm^{-1} more than in $Ti^+(CH_4)_3$. The spectra of the $M^+(CH_4)_4$ are also similar, and neither has a peak near 3000 cm^{-1}, indicating that the CH_4 all bind in an η^2 orientation. However, the $Ti^+(CH_4)_4$ spectrum has one broad peak, while the peak in the $Zr^+(CH_4)_4$ spectrum is a doublet, with resolved contributions from the symmetric and antisymmetric proximate C−H stretches. The $Zr^+(CH_4)_4$ and $Ti^+(CH_4)_4$ symmetric stretch peaks are within 15 cm^{-1} of each other.

The symmetric C−H stretches of $Ti^+(CH_4)(Ar)$ to $Ti^+(CH_4)_4$ are red shifted 149, 152, 128, and 107 cm^{-1} from the symmetric stretch in bare CH_4. Generally, these shifts decrease with increasing CH_4 around the metal, however, this is not the case with Zr^+. The symmetric C−H stretches of $Zr^+(CH_4)(Ar)$ to $Zr^+(CH_4)_4$ are red shifted 134, 147, 170, and 122 cm^{-1}, respectively.

The entrance channel complexes $M^+(CH_4)_n$ for M=Ti and Zr have very similar geometries. The $M^+(CH_4)(Ar)$ and $M^+(CH_4)_2$ complexes have η^3 methane coordination and the heavy atoms are collinear. In both of the n=2 complexes the CH_4 molecules are staggered by 60°. The calculated structures of the n=3 complexes are similar. In each case, there are two CH_4 with relatively short r_{M-C} and hydrogen coordination between η^2 and η^3. The third CH_4 has significantly longer r_{M-C} and η^2 coordination. In each case, the spectrum is consistent with a structure in which the methanes interconvert rapidly. For both metals, the n=4 complexes have a distorted square planar structure, with two different M−C bond lengths

and η^2 methane coordination. The presence of two peaks in the proximate C−H stretching region for $Zr^+(CH_4)_4$ and one for $Ti^+(CH_4)_4$ suggests that the methanes interconvert more slowly in the Zr^+ complex.

In their study of the reactions of Ti^+ with CH_4, van Koppen *et al.*[25] observe C−H bond activation and loss of H_2 following addition of the third methane, but only at temperatures >500 K. They propose that this reaction is due to sequential addition of methanes to Ti^+, with incomplete cooling, so that the addition of the third methane results in a $Ti^+(CH_4)_3$ complex which has sufficient internal energy to overcome the barrier to C−H bond activation. Our results are consistent with this suggestion. We do not observe dehydrogenation from the sequential reactions of Ti^+ with methane, even if the reactions are carried out under "hot" conditions (high ablation laser fluence and low backing pressure). However, the reactions in our ion source are taking place at pressures ∼100x higher than those used in the van Koppen study and with methane diluted in helium, so methane adducts are quickly cooled. Previous studies have shown that Zr^+ is more reactive with hydrocarbons than Ti^+[12,14] and we do observe dehydrogenation products when Zr^+ sequentially reacts with three or four CH_4.[33] Vibrational spectroscopy of $[Zr,C_n,H_{4n}]^+$ (n=1,2) shows that C−H bond activation occurs, forming $(H_2)ZrCH_2^+(CH_4)_{n-1}$ exit channel complexes, in addition to $Zr^+(CH_4)_n$ entrance channel complexes.[33]

3.3 $V^+(CH_4)_n$

The experimental spectra of $V^+(CH_4)(Ar)$ and $V^+(CH_4)_n$ (n=2-4) in Figure 7 show peaks to the red of the symmetric and antisymmetric C−H stretches in bare CH_4 (2917 and 3019 cm^{-1}) and a peak around 3000 cm^{-1} for n=1-2 which then disappears for n=3-4.

3.3.1 $V^+(CH_4)(Ar)$

No photodissociation is observed for $V^+(CH_4)$, which has a measured[41] binding energy of 5250 ± 300 cm^{-1}, and a calculated binding energy of 5405 cm^{-1} (Table 3), so an Ar tag was

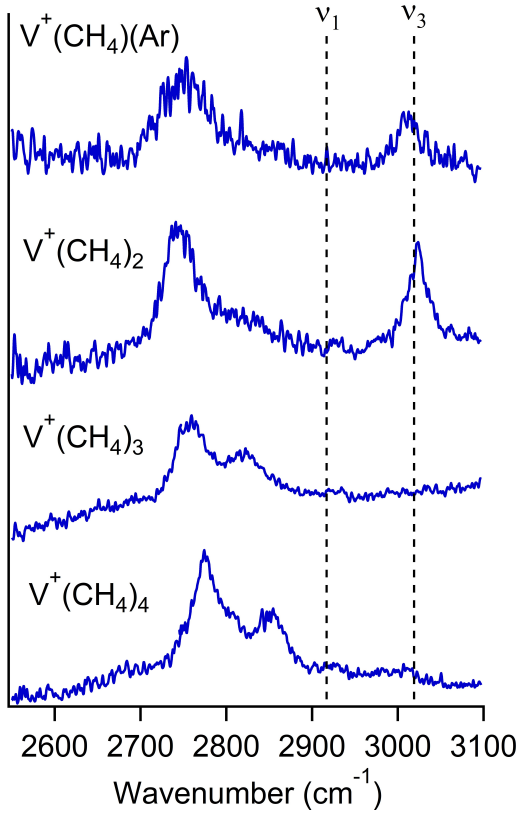

Figure 7: Vibrational spectra of $V^+(CH_4)(Ar)$ and $V^+(CH_4)_n$ n=2-4 in the C−H stretching region 2550-3100 cm^{-1}. The symmetric (ν_1) and antisymmetric (ν_3) stretches in bare CH_4 are shown by the dotted vertical lines. The y-axis shows the normalized photofragment yield.

Table 3: Experimental and calculated binding energies of $V^+(CH_4)(Ar)$ and $V^+(CH_4)_n$ n=1-4[a]

Species	cm^{-1}	kJ/mol	exp (kJ/mol)
V^+-CH_4	5405	64.7	62.8±3.6[b]
V^+CH_4-Ar	2790	33.4	
$V^+CH_4-CH_4$	4979	59.6	
$V^+(CH_4)_2-CH_4$	2693	32.2	
$V^+(CH_4)_3-CH_4$	2606	31.2	

[a]Calculations are at zero Kelvin at the B3LYP/6-311++G(3df,3pd) level of theory. [b]Ref.[41]

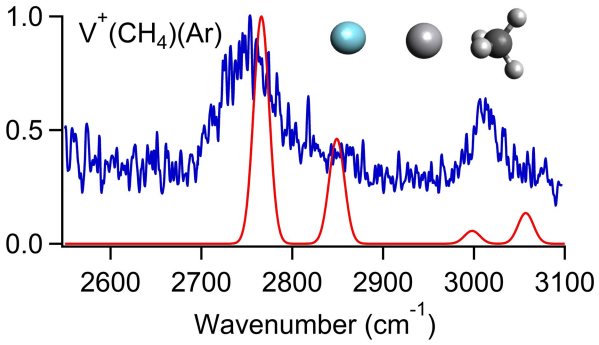

Figure 8: Experimental photodissociation spectrum (blue), simulated spectrum (red), and the optimized geometry of $V^+(CH_4)(Ar)$ at the B3LYP/6-311++G(3df,3pd) level of theory.

used to take the spectrum in Figure 8. The ground state of V^+ is a quintet and it remains a quintet with the addition of Ar and at least four CH_4. The calculations for $V^+(CH_4)(Ar)$ predict the Ar−V−C atoms are collinear and the CH_4 has η^2 hydrogen coordination. The predicted V−C bond length is 2.495 Å, which is 0.017 Å longer than in the untagged complex. The untagged and tagged simulated spectra are very similar, so the Ar has a minimal effect on the spectrum.

The experimental spectrum has a broad peak at 2753 cm^{-1} and a less intense peak at 3013 cm^{-1}. The simulated spectrum has two peaks at 2766 and 2849 cm^{-1} which correspond to the proximate symmetric and the antisymmetric C−H stretches. There are two weak peaks at 2998 and 3057 cm^{-1}, due to the distal symmetric and antisymmetric stretches. The spectrum is very similar to those measured by Xu *et al.* for $V_5O_{12}{}^+(CH_4)$ and $V_5O_{13}{}^+(CH_4)$, which have peaks at ∼2770 cm^{-1} and ∼2990 cm^{-1} and in which the methane is also predicted to bind to vanadium with η^2 hydrogen coordination.[58]

3.3.2 $V^+(CH_4)_2$

The spectrum of $V^+(CH_4)_2$ (Figure 9) is obtained by IRMPD because the second methane is bound by 4979 cm^{-1}. The experimental spectrum has an intense peak at 2742 cm^{-1} with a shoulder near 2830 cm^{-1} and a sharp peak at 3016 cm^{-1}. The calculation predicts that the C−V−C atoms are collinear with r_{V-C}=2.370 Å. The methane hydrogen coordination is

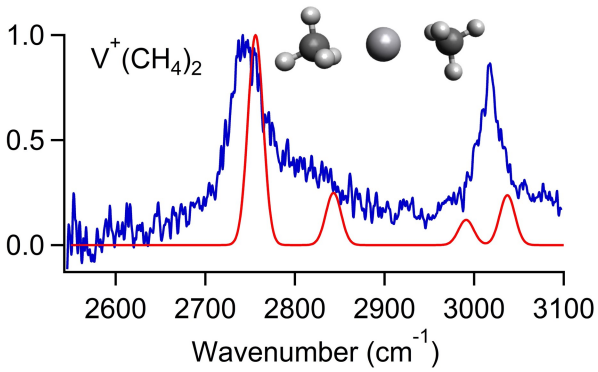

Figure 9: Experimental photodissociation spectrum (blue), simulated spectrum (red), and the optimized geometry of $V^+(CH_4)_2$ at the B3LYP/6-311++G(3df,3pd) level of theory.

between η^2 and η^3, with $\angle$H−C−V=156°. The simulated spectrum predicts two peaks at 2756 and 2843 cm^{-1} due to the proximate symmetric and antisymmetric C−H stretches and two weaker peaks at 2991 and 3037 cm^{-1} from the distal symmetric and antisymmetric stretches. The experimental symmetric stretch peak is slightly more red shifted than predicted (∼14 cm^{-1}) and the tailing is likely due to the antisymmetric stretch. The simulation does not provide a good match to the single, rather intense experimental peak at 3016 cm^{-1}. This is likely because the simulated spectrum is only calculated at the minimum energy geometry. Because the methane coordination is roughly halfway between η^2 and η^3, the η^2 and η^3 configurations are at quite low energy and it is likely that both are sampled experimentally. Figure S4 shows spectra with the molecule constrained to η^2 and η^3 methane hydrogen coordination, which are at a relative energy of 406 and 234 cm^{-1}, respectively. Configurations for η^2 are predicted to yield a weak doublet near 3000 cm^{-1}, while those for η^3 produce an intense peak near 3030 cm^{-1}, so dynamical configurations near η^3 coordination contribute more strongly to this region of the spectrum.

3.3.3 $V^+(CH_4)_3$

The experimental spectrum of $V^+(CH_4)_3$, shown in Figure 10, has two peaks at 2759 and 2822 cm^{-1} on top of a monotonically increasing non-resonant dissociation signal. The third methane is calculated to bind by 2693 cm^{-1}, which is much smaller than the first two

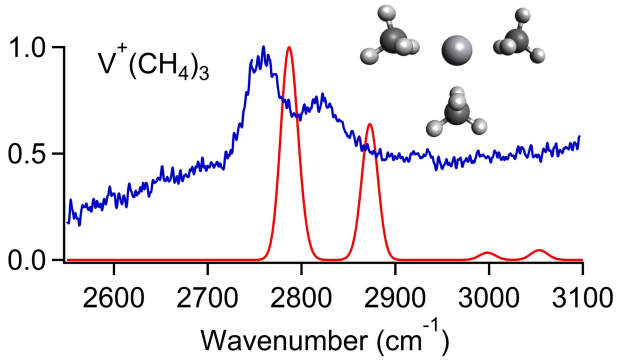

Figure 10: Experimental photodissociation spectrum (blue), simulated spectrum (red), and the optimized geometry of $V^+(CH_4)_3$ at the B3LYP/6-311++G(3df,3pd) level of theory.

methanes. The simulation predicts a trigonal planar geometry with C_{2v} symmetry and two nearly η^2 ($\angle$H−C−V=135°; r_{V-C}= 2.533 Å) and one η^2 methane ($\angle$H−C−V=125°; r_{V-C}= 2.555 Å). The simulation predicts two intense peaks, at 2787 and 2873 cm^{-1}; the former peak encompasses three nearly degenerate vibrations of the proximate C−H symmetric stretch and the latter peak is the corresponding antisymmetric stretches. The calculations predict a smaller red shift than is observed, by 28 and 51 cm^{-1}, respectively. The lack of observed peaks near 3000 cm^{-1} is consistent with η^2 hydrogen coordination. The non-resonant dissociation is likely due to a transition to a low-lying excited electronic state.

3.3.4 $V^+(CH_4)_4$

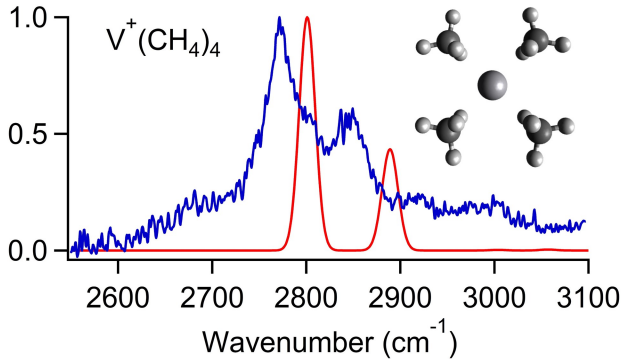

Figure 11: Experimental photodissociation spectrum (blue), simulated spectrum (red), and the optimized geometry of $V^+(CH_4)_4$ at the B3LYP/6-311++G(3df,3pd) level of theory.

The $V^+(CH_4)_4$ experimental and simulated spectra are similar to those of $V^+(CH_4)_3$. The experimental spectrum (Figure 11) has two peaks at 2771 and 2845 cm^{-1}. The fourth methane is bound by 2606 cm^{-1}, similar to the binding strength of the third methane and much less than the first two. The calculations predict a square planar geometry with D_{4h} symmetry, η^2 hydrogen coordination, and r_{V-C}= 2.580 Å. Again, the calculation underpredicts the red shift in the proximate symmetric and antisymmetric C−H stretches, with calculated peaks at 2801 and 2889 cm^{-1}

The symmetric C−H stretches of $V^+(CH_4)(Ar)$ to $V^+(CH_4)_4$ are red shifted 164, 175, 158, and 146 cm^{-1}, respectively, from the stretch in bare CH_4. Compared to other metal cation-methane complexes, $V^+(CH_4)_{1\text{-}4}$ are unusual in that the red shift barely changes as more methanes are added.

3.3.5 $Ti^+(CH_4)_n$ vs. $V^+(CH_4)_n$

The experimental spectra of the entrance channel complexes for $M^+(CH_4)(Ar)$ and $M^+(CH_4)_n$ (M=Ti,V; n=2-4) are shown together in Figure S5. The symmetric C−H stretches of $M^+(CH_4)(Ar)$ to $M^+(CH_4)_4$ are red shifted from the symmetric stretch in bare CH_4 by 149, 152, 128, and 107 cm^{-1} for titanium and 164, 175, 158, 146 cm^{-1} for vanadium. In each case, the symmetric stretch peak for the vanadium complex is red shifted more than for the titanium complex. The antisymmetric proximate C−H stretch peak is not clearly observed for titanium, but is for $V^+(CH_4)_n$ (n=3-4). The distal C−H stretch peak near 3020 cm^{-1} is present for n=1-2 for both metals and for n=3 for titanium. Neither n=4 complex has this peak, which suggests they have η^2 methane orientation.

The differences and similarities in the structures of the titanium and vanadium complexes reflect the singly-occupied molecular orbitals (SOMOs) (Figures S6 and S7). The equilibrium geometries minimize repulsive overlap between the SOMOs and the methane ligands. The ground state of Ti^+ is quartet $3d^2$ 4s, with quartet $3d^3$ at 10.3 kJ/mol (spin-orbit weighted average). The ground state of V^+ is quintet $3d^4$ with quintet $3d^3$ 4s at 32.5

kJ/mol. Complexes with methane lead to varying amounts of 3d-4s hybridization. Natural bond order[59] (NBO) calculations indicate 4s occupancy of 0.37 e^- for $Ti^+(CH_4)$ and $Ti^+(CH_4)_2$, dropping to ∼0.25 e^- for the larger clusters. There is slightly less 4s character for the vanadium complexes, ranging from 0.25 e^- for $V^+(CH_4)$ to 0.18 e^- for $V^+(CH_4)_4$, (Table S1). $Ti^+(CH_4)$, $Ti^+(CH_4)(Ar)$, and $Ti^+(CH_4)_2$ all have η^3 methane hydrogen coordination. In each case, the SOMOs are a degenerate pair based on d orbitals, and a $3d_{z^2}/4s$ hybrid (the orbitals and axis system for each molecule are shown in Figures S6 and S7. In contrast, $V^+(CH_4)$ and $V^+(CH_4)(Ar)$ have η^2 coordination. The three lowest-lying SOMOs are d_{xy}, d_{yz}, and d_{xz}, and the fourth orbital is a $3d_{z^2}/3d_{x^2-y^2}/4s$ hybrid. In $V^+(CH_4)$ the d_{xz} orbital points towards the proximate hydrogens. This interaction would become even more repulsive with the addition of the second methane. As a result, this orbital becomes the LUMO of $V^+(CH_4)_2$. The methanes are bent away from each other, leading to coordination intermediate between η^2 and η^3. The observation of a peak near 3020 cm^{-1} for $V^+(CH_4)_{1\text{-}2}$ is somewhat surprising, as this is typically not observed for η^2 coordination. It is likely due to dynamical inter-conversion between η^2 and η^3.

The geometries of the n=3 complexes are quite similar. Both have one η^2 methane farther from the metal and two methanes closer to the metal. For vanadium, these methanes are almost η^2 ($\angle$M−C−H=135°) and for titanium, they are between η^2 and η^3 ($\angle$M−C−H=150°). The SOMOs for these molecules are also similar. In $Ti^+(CH_4)_3$ the d_{xy}, d_{yz} and $3d_{z^2}/4s$ hybrid are singly occupied. In $V^+(CH_4)_3$, the d_{xz} is also occupied.

The n=4 complexes are also very similar in geometry. $V^+(CH_4)_4$ is square planar, with four equal V-C bond lengths while $Ti^+(CH_4)_4$ is distorted square planar, with two different Ti-C bond lengths. They both have η^2 methane coordination. The SOMOs in $V^+(CH_4)_4$ are very similar to those in $V^+(CH_4)_3$, while in $Ti^+(CH_4)_4$ the d_{xz} is singly occupied, rather than the d_{yz}. The d_{xy} and $3d_{z^2}/4s$ orbitals interact symmetrically with all of the methanes. The electron in the d_{yz} orbital repels the methanes on the y axis, while the one in the d_{xz} repels the methanes on the x axis to the same extent. Because both of these orbitals are occupied

in $V^+(CH_4)_4$, they repel equally and it adopts a square planar geometry. In $Ti^+(CH_4)_4$ the d_{yz} is not occupied, so the methanes on the y axis are closer to the metal than those on the x axis, resulting in a distorted square planar structure.

4 Conclusions

Photofragment spectroscopy is used to measure the entrance channel complexes $M^+(CH_4)(Ar)$ and $M^+(CH_4)_n$ (M=Ti,V; n=1-4) in the C−H stretching region (2550-3100 cm^{-1}). For most of the species, loss of methane is monitored to obtain the spectra; Ar is used for the Ar-tagged species. The vibrational spectra are then used in conjunction with simulations done at the B3LYP/6-311++G(3df,3pd) level of theory to determine the structure of the ions.

The spectra show peaks due to the symmetric proximate C−H stretch and the free distal C−H stretch of methane. The antisymmetric C−H stretch is also observed for $V^+(CH_4)_{3\text{-}4}$. The symmetric stretch peak of the vanadium complexes is more red shifted than in the titanium complexes. The simulated spectra indicate that the vanadium complexes favor an η^2 methane orientation, with some contributions from η^3 for $V^+(CH_4)(Ar)$ and $V^+(CH_4)_2$. The titanium complexes adopt η^3 methane orientation for $Ti^+(CH_4)(Ar)$ and $Ti^+(CH_4)_2$, mixed for $Ti^+(CH_4)_3$, and η^2 for $Ti^+(CH_4)_4$. The differences in the structures can be explained using the singly-occupied molecular orbitals.

Supporting Information Available

Full references for 44 and 46; the experimental and simulated spectra of $Ti^+(CH_4)$ (Figure S1), $V^+(CH_4)(Ar)$ (Figure S3), and $V^+(CH_4)_2$ (Figure S4); comparison of $Zr^+(CH_4)_n$ vs $Ti^+(CH_4)_n$ (Figure S2) and $Ti^+(CH_4)_n$ vs. $V^+(CH_4)_n$ (Figure S5); MOs of $Ti^+(CH_4)_n$ (Figure S6) and $V^+(CH_4)_n$ (Figure S7); NBO population analysis of $M^+(CH_4)_{1\text{-}4}$ (M=Ti,V) (Table S1); and the energies, geometries, vibrational frequencies, and intensities of each complex at the B3LYP/aug-cc-pVTZ level of theory (Tables S2 & S3).

Acknowledgement

Financial support from the National Science Foundation under award no. CHE-1856490 is gratefully acknowledged. The authors are grateful for computational resources provided by the Massachusetts Green High-Performance Computing Center (MGHPCC).

References

(1) Energy Information Administration, U. S. *Monthly Energy Review*; US Department of Energy: Washington DC, 2021; pp 45, Table 2.5.

(2) Alvarez-Galvan, M. C.; Mota, N.; Ojeda, M.; Rojas, S.; Navarro, R.; Fierro, J. L. G. Direct Methane Conversion Routes to Chemicals and Fuels. *Catal. Today* **2011**, *171*, 15–23.

(3) Jahangiri, H.; Bennett, J.; Mahjoubi, P.; Wilson, K.; Gu, S. A review of Advanced Catalyst Development for Fischer-Tropsch Synthesis of Hydrocarbons from Biomass Derived Syn-gas. *Catal. Sci. Technol.* **2014**, *4*, 2210–2229.

(4) Barton, D. H. R. The Invention of Chemical Reactions. *Aldrichim. Acta* **1990**, *23*, 3–10.

(5) Irikura, K. K.; Beauchamp, J. L. Osmium Tetroxide and its Fragment Ions in the Gas Phase: Reactivity with Hydrocarbons and Small Molecules. *J. Am. Chem. Soc.* **1989**, *111*, 75–85.

(6) Buckner, S. W.; MacMahon, T. J.; Byrd, G. D.; Freiser, B. S. Gas-Phase Reactions of Niobium$^+$ and Tantalum$^+$ with Alkanes and Alkenes. Carbon-Hydrogen Bond Activation and Ligand-Coupling Mechanisms. *Inorg. Chem.* **1989**, *28*, 3511–3518.

(7) Irikura, K. K.; Beauchamp, J. L. Electronic Structure Considerations for Methane Activation by Third-Row Transition-Metal Ions. *J. Phys. Chem.* **1991**, *95*, 8344–8351.

(8) Irikura, K. K.; Beauchamp, J. L. Methane Oligomerization in the Gas Phase by Third-Row Transition-Metal Ions. *J. Am. Chem. Soc.* **1991**, *113*, 2769–2770.

(9) Armentrout, P. B. Electronic State-Specific Transition Metal Ion Chemistry. *Annu. Rev. Phys. Chem.* **1990**, *41*, 313–344.

(10) Weisshaar, J. C. Bare Transition Metal Atoms in the Gas Phase: Reactions of M, M^+, and M^{2+} with Hydrocarbons. *Acc. Chem. Res.* **1993**, *26*, 213–219.

(11) Sievers, M.; Chen, Y.; Haynes, C.; Armentrout, P. Activation of CH_4, C_2H_6, and C_3H_8 by Gas-Phase Nb^+ and the Thermochemistry of Nb-Ligand Complexes. *Int. J. Mass Spectrom.* **2000**, *195-196*, 149–170.

(12) Armentrout, P. B.; Sievers, M. R. Activation of CH_4 by Gas-Phase Zr^+ and the Thermochemistry of Zr-Ligand Complexes. *J. Phys. Chem. A* **2003**, *107*, 4396–4406.

(13) Sievers, M. R.; Armentrout, P. B. Activation of C_2H_6, C_3H_8, and c-C_3H_6 by Gas-Phase Zr^+ and the Thermochemistry of Zr-Ligand Complexes. *Organometallics* **2003**, *22*, 2599–2611.

(14) Shayesteh, A.; Lavrov, V. V.; Koyanagi, G. K.; Bohme, D. K. Reactions of Atomic Cations with Methane: Gas Phase Room-Temperature Kinetics and Periodicities in Reactivity. *J. Phys. Chem. A* **2009**, *113*, 5602–5611.

(15) Armentrout, P. B. Methane Activation by 5d Transition Metals: Energetics, Mechanisms, and Periodic Trends. *Chem.: Eur. J.* **2017**, *23*, 10–18.

(16) Armentrout, P. B.; Kickel, B. L. In *Organometallic Ion Chemistry*; Freiser, B. S., Ed.; Kluwer: Dordrecht, 1996; pp 1–45.

(17) Roithová, J.; Schröder, D. Selective Activation of Alkanes by Gas-Phase Metal Ions. *Chem. Rev.* **2010**, *110*, 1170–1211.

(18) Schwarz, H., Chemistry with Methane: Concepts Rather than Recipes. *Angew. Chem. Int. Ed.* **2011**, *50*, 10096–10115.

(19) Schwarz, H., How and Why Do Cluster Size, Charge State, and Ligands Affect the Course of Metal-Mediated Gas-Phase Activation of Methane? *Isr. J. Chem.* **2014**, *54*, 1413–1431.

(20) Sunderlin, L. S.; Armentrout, P. B. Methane Activation by Ti^+: Electronic and Translational Energy Dependence. *J. Phys. Chem.* **1988**, *92*, 1209–1219.

(21) Aristov, N.; Armentrout, P. B. Methane Activation by V^+: Electronic and Translational Energy Dependence. *J. Phys. Chem.* **1987**, *91*, 6178–6188.

(22) Ng, C. Y.; Xu, Y.; Chang, Y. C.; Wannenmacher, A.; Parziale, M.; Armentrout, P. B. Quantum Electronic Control on Chemical Activation of Methane by Collision with Spin-orbit State Selected Vanadium Cation. *Phys. Chem. Chem. Phys.* **2021**, *23*, 273–286.

(23) Tonkyn, R.; Ronan, M.; Weisshaar, J. C. Multicollision Chemistry of Gas-Phase Transition-metal Ions with Small Alkanes: Rate Constants and Product Branching at 0.75 Torr of He. *J. Phys. Chem.* **1988**, *92*, 92–102.

(24) van Koppen, P. A. M.; Kemper, P. R.; Bushnell, J. E.; Bowers, M. T. Methane Dehydrogenation by Ti^+: A Cluster-Assisted Mechanism for σ-Bond Activation. *J. Am. Chem. Soc.* **1995**, *117*, 2098–2099.

(25) van Koppen, P. A. M.; Perry, J. K.; Kemper, P. R.; Bushnell, J. E.; Bowers, M. T. Activation of Methane by Ti^+: A Cluster Assisted Mechanism for σ-Bond Activation, Experiment, and Theory. *Int. J. Mass Spectrom.* **1999**, *185-187*, 989–1001.

(26) Bihlmeier, A.; Greene, T. M.; Himmel, H. J. Toward a More Detailed Understanding of Oxidative-addition Mechanisms: Combined Experimental and Quantum-chemical Study of the Insertion of Titanium Atoms into C−H, Si−H, and Sn−H Bonds. *Organometallics* **2004**, *23*, 2350–2361.

(27) Andrews, L.; Cho, H. G.; Wang, X. Reactions of Methane with Titanium Atoms: CH_3TiH, $CH_2{=}TiH_2$, Agostic Bonding, and $(CH_3)_2TiH_2$. *Inorg. Chem.* **2005**, *44*, 4834–4842.

(28) Cho, H. G.; Andrews, L. Methane Activation by Laser-ablated V, Nb, and Ta Atoms: Formation of $CH_3{-}MH$, $CH_2{=}MH_2$, $CH{\equiv}MH_3^-$, and $(CH_3)_2MH_2$. *J Phys. Chem. A* **2006**, *110*, 3886–3902.

(29) Rodriguez, O.; Lisy, J. M. Infrared Spectroscopy of $Li^+(CH_4)_1Ar_n$, n=1-6, Clusters. *J. Phys. Chem. A* **2011**, *115*, 1228–1233.

(30) Rodriguez, O.; Lisy, J. M. Infrared Spectroscopy of $Li^+(CH_4)_n$, n=1-9, Clusters. *Chem. Phys. Lett.* **2011**, *502*, 145–149.

(31) Poad, B.; Thompson, C.; Bieske, E. Infrared Spectra of Mass-Selected Al^+-$(CH_4)_n$ n=1-6 Clusters. *Chem. Phys.* **2008**, *346*, 176–181.

(32) Dryza, V.; Bieske, E. J. Infrared Spectra and Density Functional Theory Calculations for Mn^+-(CH_4)n (n=1-6) Clusters. *Int. J. Mass spectrom.* **2010**, *297*, 46–54.

(33) Kozubal, J.; Heck, T.; Metz, R. B. Vibrational Spectroscopy of Intermediates and C-H Activation Products of Sequential Zr^+ Reactions with CH_4. *J. Phys. Chem. A* **2020**, *124*, 8235–8245.

(34) Citir, M.; Altinay, G.; Austein-Miller, G.; Metz, R. B. Vibrational Spectroscopy and Theory of $Fe^+(CH_4)_n$ (n=1-4). *J. Phys. Chem. A* **2010**, *114*, 11322–11329.

(35) Kocak, A.; Sallese, Z.; Johnston, M. D.; Metz, R. B. Vibrational Spectroscopy of $Co^+(CH_4)_n$ and $Ni^+(CH_4)_n$ (n=1-4). *J. Phys. Chem. A* **2014**, *118*, 3253–3265.

(36) Kocak, A.; Ashraf, M. A.; Metz, R. B. Vibrational Spectroscopy Reveals Varying Structural Motifs in $Cu^+(CH_4)_n$ and $Ag^+(CH_4)_n$ (n=1-6). *J. Phys. Chem. A* **2015**, *119*, 9653–9665.

(37) Wheeler, O. W.; Salem, M.; Gao, A.; Bakker, J. M.; Armentrout, P. B. Activation of C−H Bonds in $Pt^+ + xCH_4$ Reactions, where x=1-4: Identification of the Platinum Dimethyl Cation. *J. Phys. Chem. A* **2016**, *120*, 6216–6227.

(38) Gentleman, A. S.; Green, A. E.; Price, D. R.; Cunningham, E. M.; Iskra, A.; Mackenzie, S. R. Infrared Spectroscopy of $Au^+(CH_4)_n$ Complexes and Vibrationally-Enhanced C−H Activation Reactions. *Top. Catal.* **2018**, *61*, 81–91.

(39) Cheng, Y. C.; Chen, J.; Ding, L. N.; Wong, T. H.; Kleiber, P. D.; Liu, D. Photodissociation Spectroscopy of $MgCH_4^+$. *J Chem. Phys.* **1996**, *104*, 6452–6459.

(40) Chen, J.; Cheng, Y. C.; Kleiber, P. D. Photodissociation Spectroscopy of $CaCH_4^+$. *J Chem. Phys.* **1997**, *106*, 3884–3890.

(41) Hayes, T.; Bellert, D.; Buthelezi, T.; Brucat, P. The Photodissociation of $V^+ \cdot CH_4$. *Chem. Phys. Lett.* **1997**, *264*, 220–224.

(42) Lu, W. Y.; Wong, T. H.; Kleiber, P. Photochemistry of $Zn^+(CH_4)$. *Chem. Phys. Lett.* **2001**, *347*, 183–188.

(43) Husband, J.; Aguirre, F.; Ferguson, P.; Metz, R. B. Vibrationally Resolved Photofragment Spectroscopy of FeO^+. *J. Chem. Phys.* **1999**, *111*, 1433–1437.

(44) Kocak, A.; Austein-Miller, G.; Pearson, W. L.; Altinay, G.; Metz, R. B. Dissociation Energy and Electronic and Vibrational Spectroscopy of $Co^+(H_2O)$ and Its Isotopomers. *J. Phys. Chem. A* **2013**, *117*, 1254–1264.

(45) Gordon, I. E.; Rothman, L. S.; Hill, C.; Kochanov, R. V.; Tan, Y.; Bernath, P. F.; Birk, M.; Boudon, V.; Campargue, A.; Chance, K. V. et al. The HITRAN2016 Molecular Spectroscopic Database. *J. Quant. Spectrosc. Radiat. Transfer* **2017**, *203*, 3–69.

(46) Kaur, D.; de Souza, A. M.; Wanna, J.; Hammad, S. A.; Mercorelli, L.; Perry, D. S. Multipass Cell for Molecular Beam Absorption Spectroscopy. *Appl. Opt.* **1990**, *29*, 119–124.

(47) Frisch, M. J.; Trucks, G. W.; Schlegel, H. B.; Scuseria, G. E.; Robb, M. A.; Cheeseman, J. R.; Scalmani, G.; Barone, V.; Mennucci, B.; Petersson, G. A. et al. Gaussian09 Revision D.01. 2013; Gaussian Inc. Wallingford CT.

(48) Peverati, R.; Truhlar, D. G. M11-L: A Local Density Functional That Provides Improved Accuracy for Electronic Structure Calculations in Chemistry and Physics. *J. Phys. Chem. Lett.* **2012**, *3*, 117–124.

(49) Elkind, J. L.; Armentrout, P. B. Effect of Kinetic and Electronic Energy on the Reactions of Ti^+ with H_2, HD and D_2. *Int. J. Mass Spectrom.* **1988**, *83*, 259–284.

(50) Bushnell, J. E.; Maître, P.; Kemper, P. R.; Bowers, M. T. Binding Energies of $Ti^+(H_2)_{1\text{-}6}$ Clusters: Theory and Experiment. *J. Chem. Phys.* **1997**, *106*, 10153–10167.

(51) Sunderlin, L. S.; Armentrout, P. B. Methane Activation by Ti^+: Electronic and Translational Energy Dependence. *J. Phys. Chem.* **1988**, *92*, 1209–1219.

(52) Sunderlin, L. S.; Armentrout, P. B. Thermochemistry of Ti^+-Hydrocarbon Bonds: Translational Energy Dependence of the Reactions of Ti^+ with Ethane, Propane, and Trans-2-Butene. *Int. J. Mass Spectrom.* **1989**, *94*, 149–177.

(53) Bushnell, J. E.; Kemper, P. R.; Bowers, M. T. Spin Change Induced in Vanadium(I) by Low-Field Ligands: Binding Energies of $V^+(H_2)_n$ Clusters (n=1-7). *J. Phys. Chem.* **1993**, *97*, 11628–11634.

(54) Aristov, N.; Armentrout, P. B. Reaction Mechanisms and Thermochemistry of $V^+ + C_2H_{2p}$ (p=1,2,3). *J. Am. Chem. Soc.* **1986**, *108*, 1806–1819.

(55) Ruscic, B.; Bross, D. H. ATcT Thermochemical Values ver. 1.122 of the Thermochemical Network. 2019; `https://atct.anl.gov/ThermochemicalData/version1.122/index.php`, Date Accessed February 5, 2021.

(56) Armentrout, P. B. Guided Ion Beam Studies of Transition Metal-Ligand Thermochemistry. *Int. J. Mass Spectrom.* **2003**, *227*, 289–302.

(57) Sicilia, E.; Russo, N. Theoretical Study of Ammonia and Methane Activation by First-Row Transition Metal Cations M^+ (M = Ti, V, Cr). *J. Am. Chem. Soc.* **2002**, *124*, 1471–1480.

(58) Xu, B.; Zhao, Y. X.; Ding, X. L.; Liu, Q. Y.; He, S. G. Collision-Induced Dissociation and Infrared Photodissociation Studies of Methane Adsorption on $V_5O_{12}{}^+$ and $V_5O_{13}{}^+$ Clusters. *J. Phys. Chem. A* **2013**, *117*, 2961–2970.

(59) Reed, A. E.; Curtiss, L. A.; Weinhold, F. Intermolecular Interactions From a Natural Bond Orbital, Donor-acceptor Viewpoint. *Chem. Rev.* **1988**, *88*, 899–926.

Graphical TOC Entry